Quasi-Liquid Layers on Ice Crystal Surfaces Are Made Up of Two Different Phases

Gen Sazaki[a,b,1], Salvador Zepeda[a,2], Shunichi Nakatsubo[a], Makoto Yokomine[c], Yoshinori Furukawa[a]

[a] Institute of Low Temperature Science, Hokkaido University, N19-W8, Kita-ku, Sapporo 060-0819, Japan

[b] Precursory Research for Embryonic Science and Technology (PRESTO), Japan Science and Technology Agency, 4-1-8 Honcho, Kawaguchi, Saitama 332-0012, Japan

[c] Analytical Systems Department, TOYO Corporation, 1-1-6 Yaesu, Chuo-ku, Tokyo 103-8284, Japan

Author contributions: G.S. and Y.F. designed the research performed by G.S. and S.Z. S.N. produced the experimental system. M.Y. programmed the image processing software. G.S. and Y.F. wrote the paper.

The authors declare no conflict of interest.

[1] To whom correspondence should be addressed. E-mail: sazaki@lowtem.hokudai.ac.jp

[2] Present address: CCZ Crystal R&D, MEMC Electronic Materials, Inc., 501 Pearl Dr. (City of Present O'Fallon), PO Box 8, St. Peters, MO 63376, USA

This article contains supporting information online at www.pnas.org/cgi/content.full/

Classification: Major: Physical Science, Minor: Physics

Additional key words: in situ observation, laser confocal microscopy, differential interference contrast microscopy

Abstract

Ice plays crucially important roles in various phenomena due to its abundance on earth. However, revealing the dynamic behavior of quasi-liquid layers (QLLs), which governs the surface properties of ice crystals at temperatures near the melting point, remains an experimental challenge. Here we show that two types of QLL phases appear that exhibit different morphologies and dynamics. We directly visualized the two types of QLLs on ice crystal surfaces by advanced optical microscopy, which can visualize the individual 0.37 nm thick elementary steps on ice crystal surfaces. We found that they had different stabilities and different interactions with ice crystal surfaces. The two immiscible QLL phases appeared heterogeneously, moved around and coalesced dynamically on ice crystal surfaces. This picture of surface melting is quite different from the conventional picture in which one QLL phase appears uniformly on ice crystal surfaces.

\body

Introduction

Ice is one of the most abundant materials on earth, and its phase transition governs a wide variety of phenomena in nature. Surface melting is one of the first-order phase transitions that occur on ice crystal surfaces, and dominates the surface properties of ice crystals at temperatures below the melting point(1-3). It is generally acknowledged that quasi-liquid layers (QLLs) formed by surface melting play crucially important roles in the slipperiness of a skating rink, regelation (pressure-induced change in freezing), frost heave by ice columns, recrystallization and coarsening of ice grains, morphological change of snow crystals, cryopreservation, electrification of thunderclouds. Hence, the molecular-level understanding of QLLs holds the key to unlocking the secrets of those phenomena.

Although surface melting was first proposed by M. Faraday in the 1850s(4), it was not until the mid-1980s that QLLs on ice crystal surfaces could be measured experimentally(1). Since then, many studies have measured the thickness of QLLs as a function of temperature by various methods(1-3) (Supplementary table S1). All those studies reported that the thickness of QLLs increased significantly with increasing temperature, however their results showed considerable variations - as much as two orders of magnitude - depending on both measurement methods and researchers(1, 3, 5). Such variations could partly result from a lack of spatial and temporal resolution and variations in ice samples. To effectively study QLLs on ice crystal surfaces, the technique used needs to have sufficient spatial and temporal resolution.

We and Olympus Engineering Co. Ltd. have developed one such technique, namely laser confocal microscopy combined with differential interference contrast microscopy (LCM-DIM)(6), which can directly visualize the 0.37 nm thick elementary steps on ice crystal surfaces with a typical frame rate of 0.1-4 s/frame(7). In this study, we directly visualized surface melting processes on ice crystal surfaces to elucidate the dynamic behavior of QLLs, and found that QLLs are made up of two different phases (fig. S1).

Results and Discussion

We grew Ih ice single crystals on an AgI crystal from supersaturated water vapor in a nitrogen environment (fig. S2). To supply water vapor to the sample ice crystals, we prepared other ice crystals (as a source of water vapor) on a separate copper plate. By separately changing the temperatures of the sample and source ice crystals, we adjusted the growth temperature of the sample ice crystals and the supersaturation of water vapor

independently. After we prepared sample ice crystals at a growth temperature of -15.0°C, we increased the temperature to a final -0.1°C, at rates of ~0.1°C/min (from -15.0 to -2.0°C) and ~0.02 °C/min (from -2.0 to -0.1°C). All through this process, we kept the sample ice crystals growing, by carefully changing the supersaturation and confirming the growth by LCM-DIM observations. Then we observed the behavior of QLLs on the surfaces of sample ice crystals. LCM-DIM images were processed according to the recipe explained in fig. S3.

Fig. 1 shows the surface morphology of a basal {0001} face of a sample ice crystal. At -0.6°C (Fig. 1A), we could observe "elementary steps"(7) (the growing ends of ubiquitous molecular layers with the minimum height: fig. S4). This result demonstrates that at -0.6°C, the basal face was flat at the molecular level and was growing layer by layer. In Fig 1A, elementary steps (a black arrowhead) grew from left to right (a black arrow).

At -0.4°C (Fig. 1B), round objects (a white arrowhead) appeared. Then, at -0.3°C (Fig. 1C), the number of the round objects increased, and their size also grew. In Fig. 1, the differential interference contrast was adjusted as if the ice crystal surface was illuminated by a light beam slanted from the upper left to the lower right direction, as explained in fig. S5. Hence, the upper-left and lower-right halves of the round objects appeared white and black, respectively.

These round objects coalesced just like liquid drops (Fig. 2 and video S1). Since the round objects were formed below 0°C, they were QLLs formed by surface melting. Hence, hereafter, we name these round objects "α-QLLs".

In 1993, Elbaum and coworkers(5) observed, by optical interference microscopy, that round drops appeared and coalesced at -0.4 to -0.2°C on basal faces of ice crystals in water vapor. Later, Gonda and Sei(8) also observed the appearance of round drops at -0.12°C by differential interference contrast microscopy. The round drops reported in these studies probably correspond to α-QLLs. In this study, in addition to the appearance of α-QLLs, we found that the elementary steps appeared around α-QLLs (marked by a black arrowhead in Fig. 1C), showing that the α-QLLs function as sources of steps (video S1).

We measured the three-dimensional geometry of an α-QLL using a He-Ne laser (633 nm), as shown in Fig. 1D. The interferogram shows that the shape of the α-QLL was a part of a sphere. The spacing between adjacent interference fringes corresponds to a height difference of a half-wavelength. Hence, the α-QLL, marked by a white arrowhead, had a

width of 50 μm and a height of 0.5 μm. Although we identified an α-QLL as a "droplet", its height/width ratio is very small (~1/100). This result indicates that solid water (ice) and liquid water showed very high wettability, strongly supporting the fact that the α-QLLs functioned as step sources.

Fig. 3 shows the surface morphology observed after we further increased the temperature. At -0.2°C, a thin layer (a red arrowhead) newly appeared (Fig. 3A). α-QLLs were generated from this thin layer and also from the crystal surface. Then, we further increased the temperature to -0.1°C (Figs. 3B-D and video S2). We could observe that elementary steps, which exhibited bright contrast (black arrowheads), advanced to the left direction. This result confirms that one portion of the crystal surface grew, demonstrating that the temperature of the crystal surface was surely below 0°C. Therefore, we could conclude that the surface melting observed in the other portion of the crystal surface occurred below 0°C. The thin layer eventually covered the whole crystal surface (Fig. 3D).

The differential interference contrast of the thin layer was significantly higher than that of an elementary step (Fig. 3). Hence, the thickness of the thin layer was much higher than that of an elementary step. We also tried to measure the thickness of the thin layer by interferometry. However we could not distinguish interference fringes, indicating that the thickness of the thin layer was smaller than the detection limit of interferometry (≤several 10 nm).

The temperature of the appearances of α-QLLs and the thin layers respectively varied from -1.5 to -0.4°C and from -1.0 to -0.1°C, depending on experimental runs. However, in the same run, the thin layers always appeared at a higher temperature than α-QLLs (fig. S1), and we could never find an inversion of the appearance temperatures.

The thin layer exhibited a feature that was significantly different from that of ice crystal surfaces. As shown in Fig. 4, the thin layers moved around the ice crystal surface, and then coalesced with each other, just like liquid droplets. The decrease in the number of the thin layers with increasing time was not due to Ostwald ripening, by which smaller crystals disappear and larger ones grow, but was rather due to coalescence. Such dynamic movement and coalescence, which occurred on a time scale of several 10s of seconds, indicate that the thin layer displays fluidity. These results strongly suggest that the thin layer was not a solid phase (ice) but a liquid phase that appeared below 0°C. Hence, we refer to the thin layers as β-QLLs.

To prove that a β-QLL was not solid, we carried out further in-situ observations. In Fig.

5A, an α-QLL is located at the center, and a β-QLL exists around the α-QLL. On a bare surface of the ice crystal, we could observe the growth of elementary steps (in black arrow directions). We found that further extreme adjustment of the gain and offset of the image enabled us to visualize elementary steps even "beneath the β-QLL" (black arrowheads) in Fig. 5B. As shown in Figs. 5B and C (video S3), we could observe the advancement of elementary steps even beneath the β-QLL (black arrowheads indicate the movement of the same step).

There are two possibilities (shown schematically in Fig. 5D) that could explain these images. The first is that elementary steps could be directly visualized through the β-QLL. The second is that elementary steps could not be visualized directly, but the deformation of the β-QLL due to the advancement of the steps could be visualized. In the first case, the refractive index of the β-QLL has to be different from that of solid ice. Hence, the β-QLL cannot be a solid phase but is a quasi-liquid phase appearing below 0°C. In the second case, the β-QLL has to be easily deformed by the lateral movement of elementary steps that are only 0.37 nm thick(7). Such an easily deformed phase would be a quasi-liquid, rather than a solid, although at present the rigidity of a solid ice film of nanometer thickness is unclear. This expectation is strongly supported by the fluidity of the β-QLL demonstrated in Fig. 4. Therefore, in either case, we concluded that we have observed the appearance of two types of QLL phases (α and β) on an ice crystal surface, as schematically summarized in Fig. 5E.

Elbaum and coworkers estimated the thickness of QLLs and the asperity of ice crystal surfaces, respectively by ellipsometry and optical interference microscopy. Then they argued that with increasing temperature, QLLs first appeared homogeneously on ice basal faces and the thickness of QLLs increased, then after the thickness of QLLs exceeded 20 nm, round drops finally appeared on QLLs. This picture is quite different from the observations made in this study: with increasing temperature, α-QLLs first appeared heterogeneously, and then β-QLLs appeared also heterogeneously, as schematically shown in Fig. 5E (also fig. S1). The different picture proposed by Elbaum et al. probably resulted from a lower spatial resolution of their observation techniques: they perhaps could not detect the heterogeneous behavior of α- and β-QLL phases in the early stages of their appearance.

We further investigated the stability of the two QLL phases. After we confirmed the appearance of α-QLLs and a β-QLL at -0.5°C, we decreased the temperature to -1.0°C, and then observed the response. Fig. 6 (video S4) shows the resulting changes. As time

elapsed, a β-QLL decomposed and changed into α-QLLs (small droplets shown in D: marked by a white arrowheads) and bunched steps. The appearance of the bunched steps (black arrowheads) means that a number of elementary steps were formed at one time (inset of Fig. 6C) by the decomposition of the β-QLL. These results demonstrate that the β-QLL was the least stable phase that appeared in the highest temperature range, with the α-QLL being more stable and forming in a lower temperature range. It is also clear that the Ih ice was most stable among the three phases, and formed in the lowest temperature range. The decrease in the size of the α-QLL located at the center (Fig. 6D) indicates that the α-QLL also partly decomposed into the most stable solid ice.

On ice crystal surfaces, β-QLLs exhibited a much flatter shape than α-QLLs, demonstrating that β-QLLs had higher wettability (more favorable interaction, i.e. smaller interfacial free energy) with ice crystal surface than α-QLLs. This result contradicts the lower stability (higher appearance temperature) of β-QLLs than α-QLLs. Resolving this contradiction will require further understanding of the physical/chemical properties of α- and β-QLLs.

In this study, we carried out in-situ observation of ice crystal surfaces by LCM-DIM. We found the appearance of two types of QLL phases (α and β) formed by surface melting below 0°C. So far, it has been thought that QLLs appear uniformly on ice crystal surfaces, and QLLs have been discussed using a static picture. However, the results found in this study demonstrate that surface melting on ice crystal surfaces proceeds through two immiscible liquid phases (α and β) that are both *dynamic and spatially inhomogeneous*. The insights into the nature of QLLs obtained from direct visualization (Fig. 5E) may play a crucially important roles in understanding a variety of phenomena in which QLLs play a vital role, from the slipperiness of a skating rink to the electrification of thunderclouds(1-3).

Materials and Methods

We attached a confocal system (FV300, Olympus Optical Corporation) to an inverted optical microscope (IX70, Olympus Optical Corporation), as previously explained(6, 7). A super luminescent diode (Amonics Ltd, model ASLD68-050-B-FA: 680 nm) and a He-Ne laser (Melles Griot 05-LHP-991: 633 nm) were used for LCM-DIM and interferometric observations, respectively. The LCM-DIM system used in this study (Fig. S2A) contained all improvements reported in our recent study(7) of the observation of elementary steps on ice crystal surfaces.

The observation chamber had upper and lower Cu plates, whose temperatures were separately controlled using Peltier elements (Fig. S2B). At the center of the upper Cu plate, a cleaved AgI crystal (a kind gift from emeritus professor G. Layton of Northern Arizona University), known as an ice nucleating agent, was attached using heat grease. On this AgI crystal, sample ice crystals were grown at -15°C. To supply water vapor to the sample ice crystals, other ice crystals were prepared on the lower Cu plate, as a source of water vapor. Other details were reported in our recent study(7). After the lateral size and height of the sample ice crystals reached several hundred μm, the temperatures of the sample and source ice crystals were increased to a final -0.1°C. During this temperature rise, QLLs that appeared on the basal faces of the sample ice crystals were observed by LCM-DIM.

To obtain the LCM-DIM images shown in this study, raw images taken by LCM-DIM were processed according to the recipe explained in Fig. S3. This image processing corrected the background intensity inhomogeneity caused by the slight misalignment of the optical axis with the surface normal of an ice crystal.

Acknowledgements

The authors thank Y. Saito and S. Kobayashi (Olympus Engineering Co., Ltd.) for their technical support of LCM-DIM, G. Layton (Northern Arizona University) for the provision of AgI crystals, and T. Sei (Aichi Gakuin University) for valuable discussions. This work was supported by Japan Science and Technology Agency PRESTO program.

References

1. Petrenko VF & Whitworth RW (1999) *Physics of ice* (Oxford University Press, Oxford).
2. Wettlaufer JS & Dash JG (2000) Melting below zero. *Scientific American* 282(2):50-53.
3. Li Y & Somorjai GA (2007) Surface premelting of ice. *Journal of Physical Chemistry C* 111(27):9631-9637.
4. Faraday M (1850) Lecture given at Royal Institution, June 7, 1850. in *reported in Athenaeum*London), p 640.
5. Elbaum M, Lipson SG, & Dash JG (1993) Optical study of surface melting on ice. *Journal of Crystal Growth* 129(3-4):491-505.
6. Sazaki G*, et al.* (2004) In situ observation of elementary growth steps on the surface of protein crystals by laser confocal microscopy. *Journal of Crystal Growth* 262(1-4):536-542.
7. Sazaki G, Zepeda S, Nakatsubo S, Yokoyama E, & Furukawa Y (2010) Elementary steps at the surface of ice crystals visualized by advanced optical microscopy. *Proceedings of the National Academy of Sciences of the United States of America* 107(46):19702-19707.
8. Gonda T, Arai T, & Sei T (1999) Experimental study on the melting process of ice crystals just below the melting point. *Polar Meteorol. Glaciol.* 13:38-42.

Figures and Legends

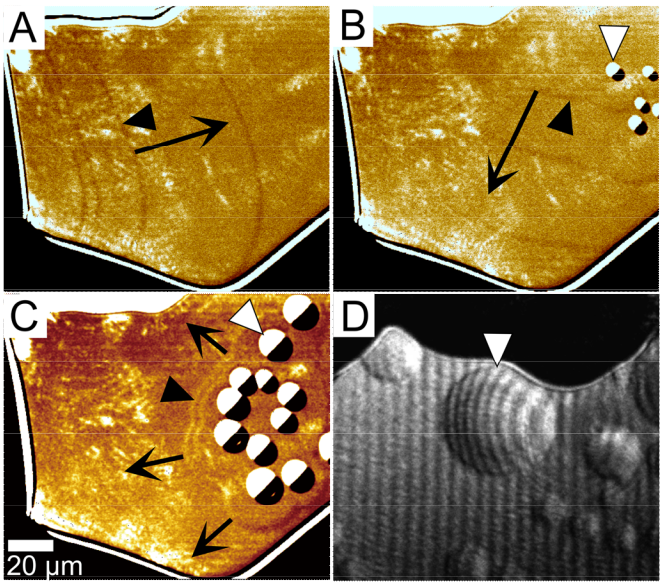

Fig. 1. The appearance of round liquid-like droplets (α-QLLs), indicated by white arrowheads, on a basal face of an ice crystal with increasing temperature. Temperature was -0.6°C (A), -0.4°C (B) and -0.3°C (C). Black arrowheads and black arrows indicate elementary steps and their growth directions, respectively. D, An interferogram of α-QLLs taken at -0.3°C using a different ice crystal during another run. A movie of the process C is available as supporting information Video S1.

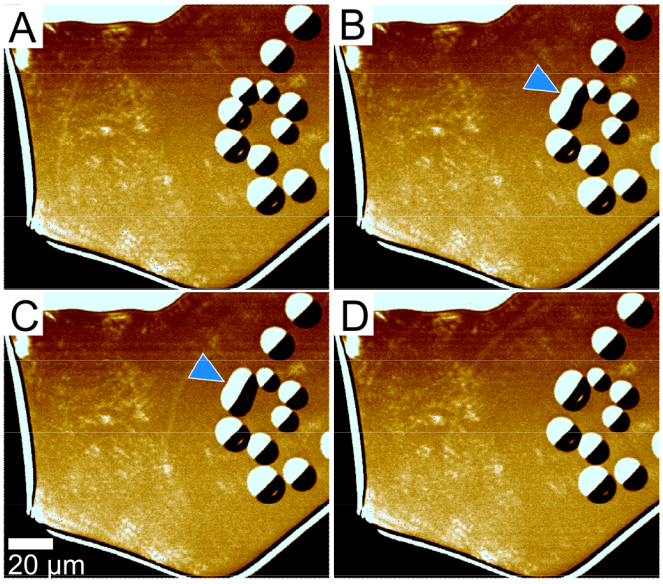

Fig. 2. The coalescence of bulk liquid-like droplets (α-QLLs) at -0.3°C. Images A-D were respectively taken 29, 30, 31 and 36 s after the temperature was set at -0.3°C. Blue arrowheads show the coalescence of α-QLLs. α-QLLs coalesced just like liquid droplets. A movie of this process is available as supporting information Video S1.

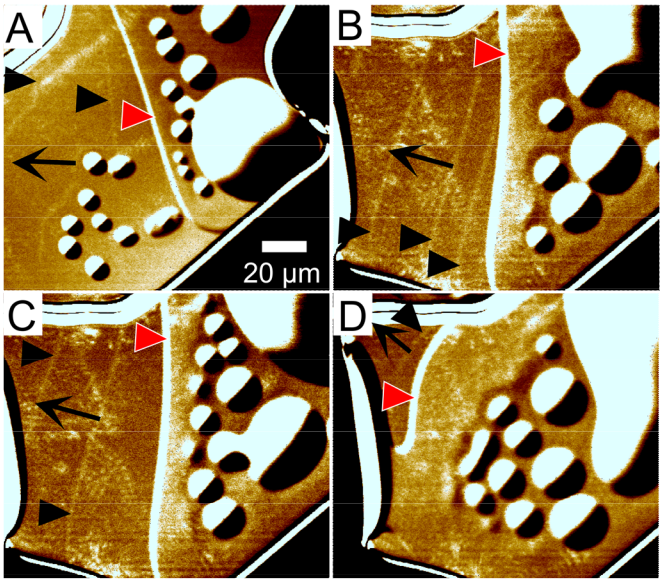

Fig. 3. The appearance of thin liquid-like layers (β-QLLs), indicated by red arrowheads, with increasing temperature. Temperature was -0.2°C (A) and -0.1°C (B, C and D). Images B, C and D were respectively taken 0, 18 and 239 s after temperature was set at -0.1°C. Other arrowheads and arrows are the same as those in Fig. 1. A movie of the process B-C is available as supporting information Video S2.

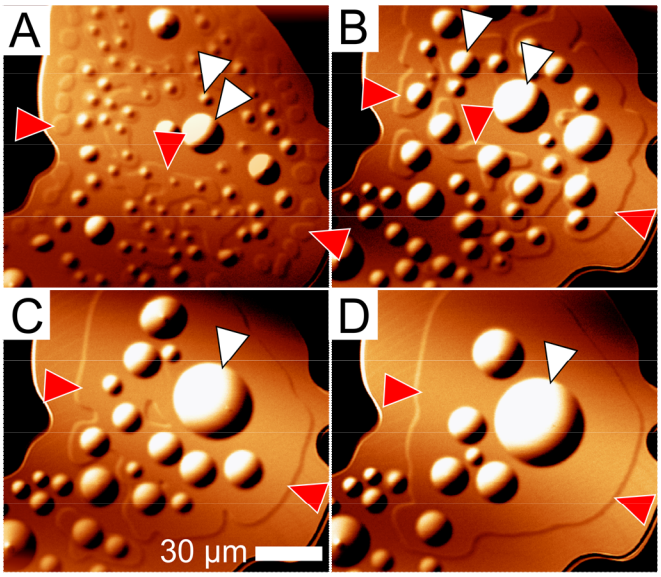

Fig. 4. The coalescence of thin liquid-like layers (β-QLLs) at -0.5°C. Images A-D were respectively taken 75, 263, 547 and 808 s after temperature was set at -0.5°C. White and red arrowheads correspond to α- and β-QLL phases, respectively. β-QLLs moved around the ice crystal surface, and then coalesced with each other just like liquid droplets. Finally, only one β-QLL was observed (D).

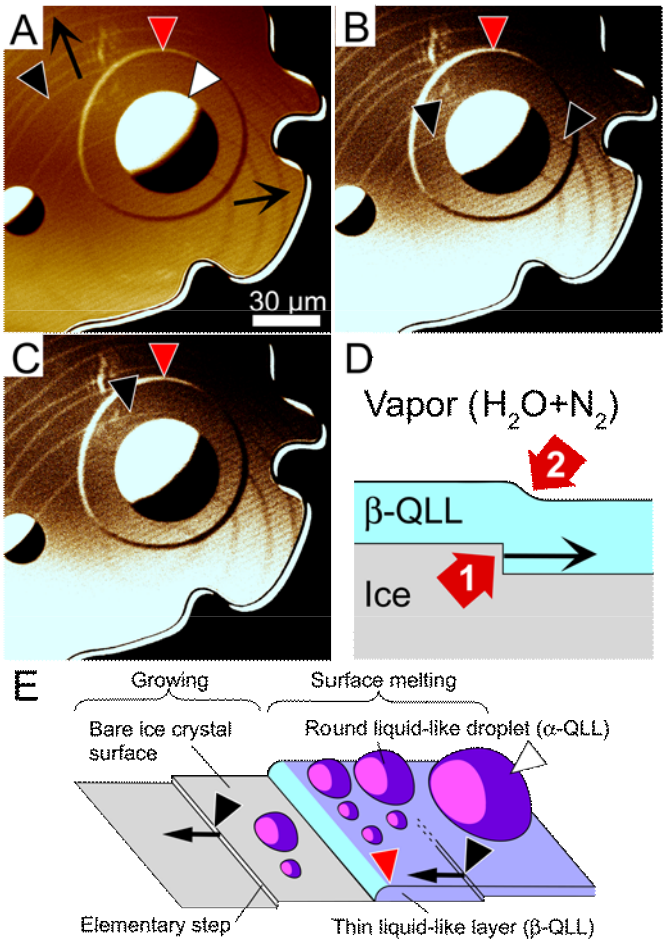

Fig. 5. Visualization of elementary steps growing beneath a thin liquid-like layer (β-QLL) at -1.0°C. The gain and offset of the image A was further extremely adjusted to obtain image B. Image C was taken 3.27 s after image B. D, A schematic cross sectional view showing two possible mechanisms (red arrows) discussed in the text for the visualization of elementary steps beneath the β-QLL. E, Schematic illustration of the appearances of two types of QLL phases (α and β). Other arrowheads and arrows are the same as those in Figs. 1 and 3. A movie of the process B-C is available as supporting information Video S3.

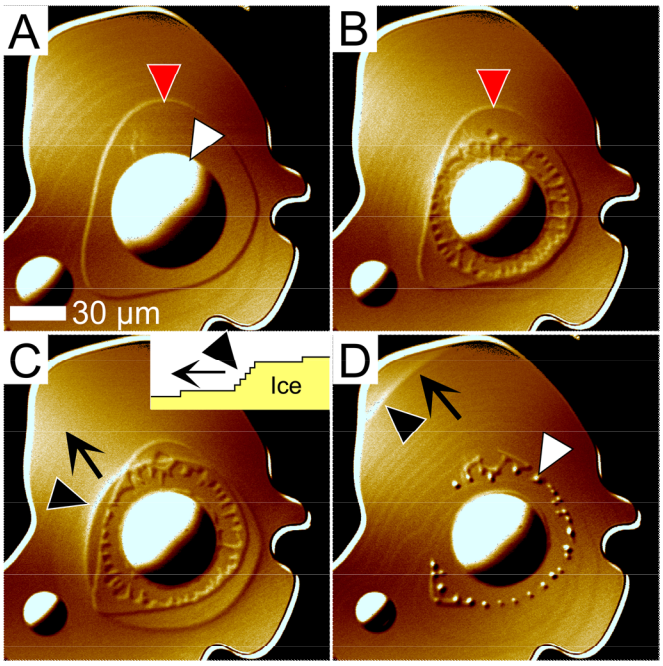

Fig. 6. Decomposition of a β-QLL into α-QLLs and solid ice with decreasing temperature. After the appearances of α-QLLs and a β-QLL were confirmed at -0.5°C, the temperature was decreased to -1.0°C. Images A-D were respectively taken 0, 20, 23 and 49 s later. In this figure, black arrowheads and black arrows respectively show bunched steps (inset of C: cross sectional view) and their growing direction. Other arrowheads and arrows are the same as those in Figs. 1-3. A movie of this process is available as supporting information Video S4.

Supporting Information

Quasi-Liquid Layers on Ice Crystal Surfaces Are Made Up of Two Different Phases

G. Sazaki*, S. Zepeda, S. Nakatsubo, M. Yokomine, Y. Furukawa

*correspondence to: sazaki@lowtem.hokudai.ac.jp

This PDF file includes:

Tables S1
Figs. S1 to S5
Captions of Videos S1 to S4
References

Other Supporting Online Material for this manuscript includes the following:

Videos S1 to S4

Table S1. Previous studies on temperature dependence measurements of the thickness of QLLs; all these studies showed a significant increase in the thickness of QLLs with increasing temperature; however, depending on the measurement methods and researchers, their results showed considerable variation - as much as two orders of magnitude; some of those variations were summarized in Fig. 1 of reference(5); there also exist many studies on QLLs by molecular dynamics and theoretical calculations, although such studies are not listed here

Measurement method	References
Proton channeling	(9, 10)
Proton back scattering	(11, 12)
Ellipsometry	(13, 14)
X-ray diffraction	(15, 16)
Glancing-angle X-ray scattering	(17, 18)
Quasi-elastic neutron scattering	(19)
Photoelectron spectroscopy	(20, 21)
Nuclear magnetic resonance	(22, 23)
Optical microscopy	(5)
Optical displacement sensor	(24)
Infrared spectroscopy	(25)
Atomic force microscopy	(26-28)

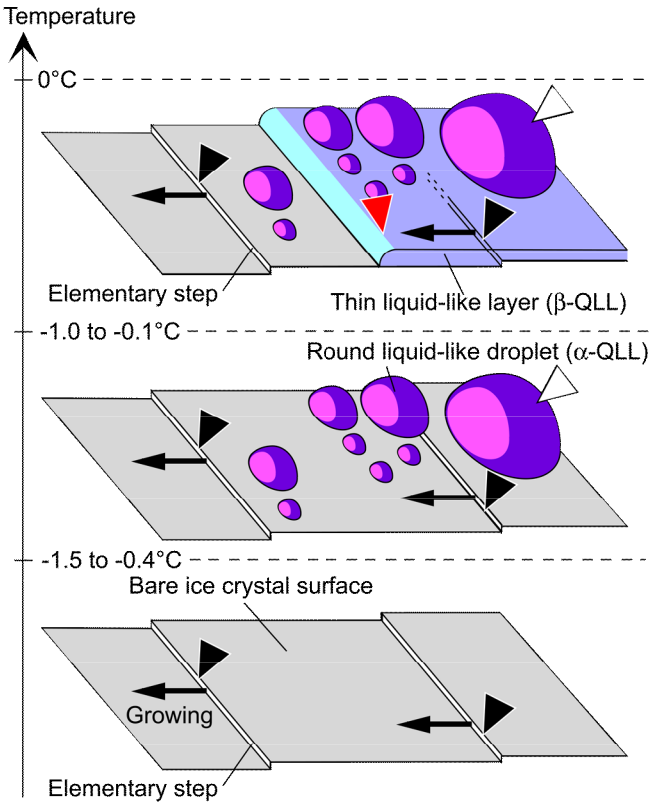

Fig. S1. Summary of the main findings of this paper. We found that two-types of QLLs appeared on a basal face of an ice crystal during surface melting. With increasing temperature, round liquid-like droplets (α-QLLs) first appeared at -1.5 to -0.4°C. In addition, we found that thin liquid-like layers (β-QLLs) appeared at -1.0 to -0.1°C. The appearance temperatures of α-QLLs and β-QLLs exhibited slight variations, but β-QLLs always appeared at a higher temperature than α-QLLs in the same run. These two QLL phases moved around and coalesced on the ice crystal surface. The different morphologies and dynamics of the two types of QLLs demonstrate that the two types of QLL phases had different interactions with ice crystal surfaces, suggesting the necessity of constructing a novel picture of surface melting. Arrowheads and arrows are the same as those in Figs. 1 and 3.

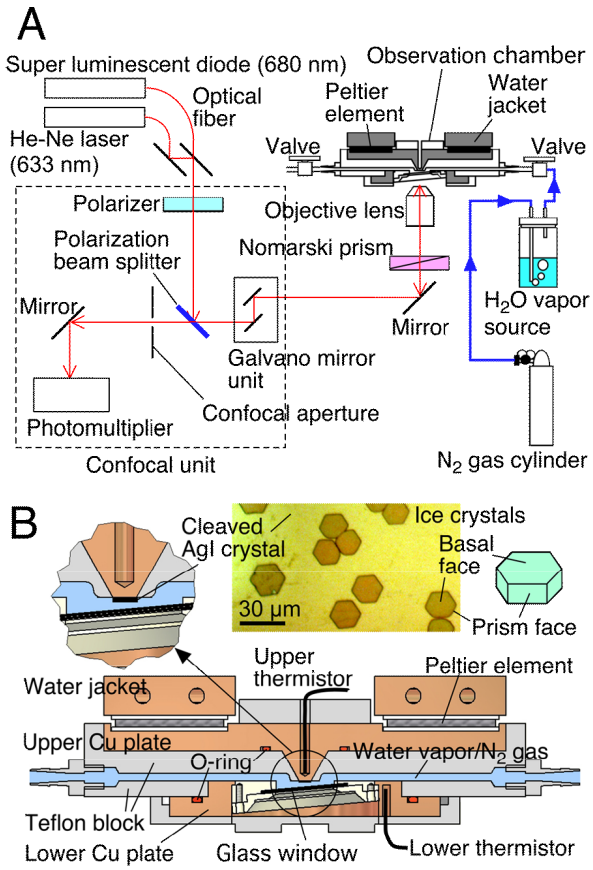

Fig. S2. Schematic drawings of the experimental setups. (A) The LCM-DIM system, the observation chamber and the water-vapor supply system; (B) a cross sectional view of the observation chamber. In B, the upper left inset shows a closeup view of the cleaved AgI crystal attached to the upper Cu plate using heat grease; the upper center inset presents a photomicrograph of Ih ice crystals grown heteroepitaxially on the AgI crystal; the upper right inset depicts the morphology of the Ih ice crystal. The surface of the cleaved AgI crystal was observed from below through a glass window that was tilted to prevent the appearance of interference fringes.

We grew Ih ice single crystals on a cleaved {0001} face of the AgI crystal from supersaturated water vapor in a nitrogen environment. We set the temperature of the ice single crystals at -15.0°C. To supply water vapor to the sample ice crystals, we prepared other ice crystals (as a source of water vapor) on the lower copper plate. By separately changing the temperatures of the upper and lower Cu plates, we adjusted the growth temperature of the sample ice crystals and the supersaturation of water vapor independently.

Sample ice crystals on the cleaved AgI crystal were ≥16 mm distant from the source ice crystals prepared on the lower Cu plate. Also the temperature of the teflon block was not controlled. Therefore, as water vapor diffused away from the source ice crystals in N_2 gas at atmospheric pressure, its temperature increased. Hence the temperature of water vapor in the vicinity of the sample ice crystals was unclear. Therefore, in our observations, the degree of supersaturation could not be quantified. However, all through the experiment, we kept the sample ice crystals growing by carefully changing the temperature of the source ice crystals and confirming the growth by LCM-DIM.

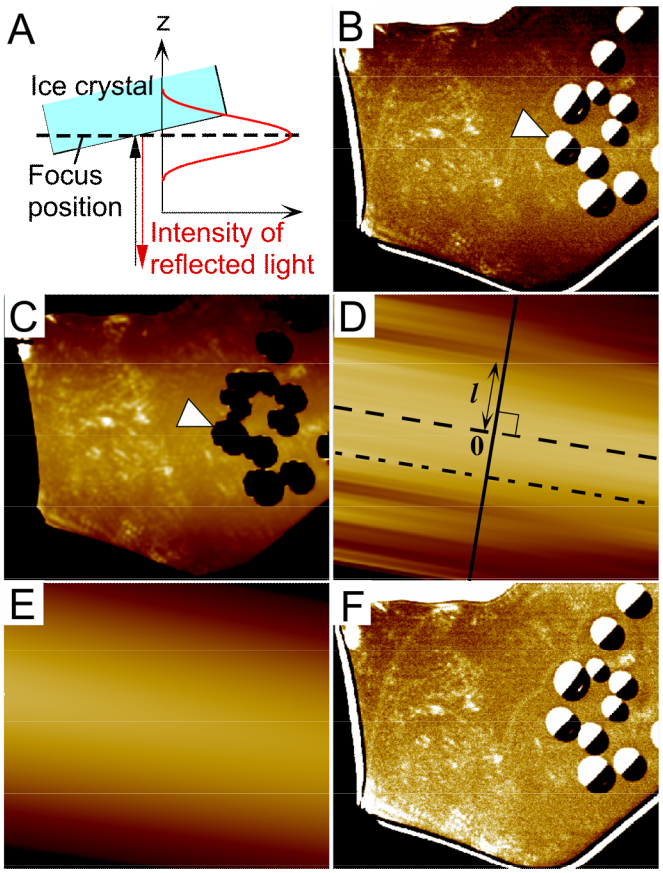

Fig. S3. The image processing performed to obtain the LCM-DIM images shown in Figs. 1 to 6. It is practically impossible to locate an ice crystal whose surface is perfectly perpendicular to the optical axis. This slight misalignment provides an inhomogeneous intensity of reflected light, as shown in A and B. In particular, in the case of confocal microscopy, the inhomogeneity of reflected light becomes significant because of its small focal depth. The area just at the focus position of an objective shows the highest intensity of reflected light. But with increasing distance from the just focused position, the intensity of reflected light significantly decreases, as A and B demonstrate. Hence, to visualize an ice crystal surface homogeneously, we corrected the inhomogeneous intensity distribution of reflected light. We obtained LCM-DIM images as a movie composed of a series of still images (4,096 gray levels) taken over a certain scan time. Then using commercial software (SPIP, Image Metrology A/S) and plug-in software (PlugIn_SnowCorr, specially written by M.Y.), we carried out the image processing as follows.

1) From the original image (B), first we eliminated the pixels whose spatial gradients of reflected light intensity were steeper than 200 gray levels/pixel as spike noise, and also removed the pixels whose reflected light intensities were higher than 4,000 gray levels, which corresponded to the areas whose gray levels were saturated (like the upper-left halves of droplets marked by white arrowheads in B and C). Then we calculated a time-averaged image (C).

2) Next, we calculated the line along which pixels had maximum intensity (dashed line shown in D). Then, along lines that were parallel to the maximum-intensity line (such as the dashed-dotted line in D), the reflected light intensities were fitted with a linear

function. During the linear fitting, only the pixels, whose gray levels were present in the range of twice the standard deviation of the intensity distribution, were calculated: i.e. the portions outside a crystal surface and inside α-QLLs were eliminated from the calculation. The image D was obtained by laying (arranging) reflected light intensities approximated by the line fittings side-by-side.

3) According to the imaging theory of confocal microscopy(29), the relation between the reflected light intensity distribution *I* and depth *z* (along the optical axis) can be expressed as (shown schematically in A)

$$I(z) = \left| \frac{\sin(kz)}{kz} \right|^2 . \quad (1)$$

Here *k* is a constant determined by the wavelength, refractive indices, and the numerical aperture of the objective. Hence, in D, the intensity distribution along the solid line that was perpendicular to the maximum dashed intensity was fitted with the following equation

$$\frac{I(l)}{I_{l=0}} = \left| \frac{\sin(a \cdot l)}{a \cdot l} \right|^2 . \quad (2)$$

Here, l is a distance along the solid line in D ($l = 0$ at the position of the dashed line), $I_{l=0}$ is the intensity at $l = 0$, $I(l)$ is the intensity at l, and a is a fitting parameter. Then we obtained the image shown in E, in which the discontinuities in intensities shown in D were smoothed.

4) Finally, we subtracted the image E from the original image B, and adjusted the gain and offset of the subtracted image to obtain the final image shown in F.

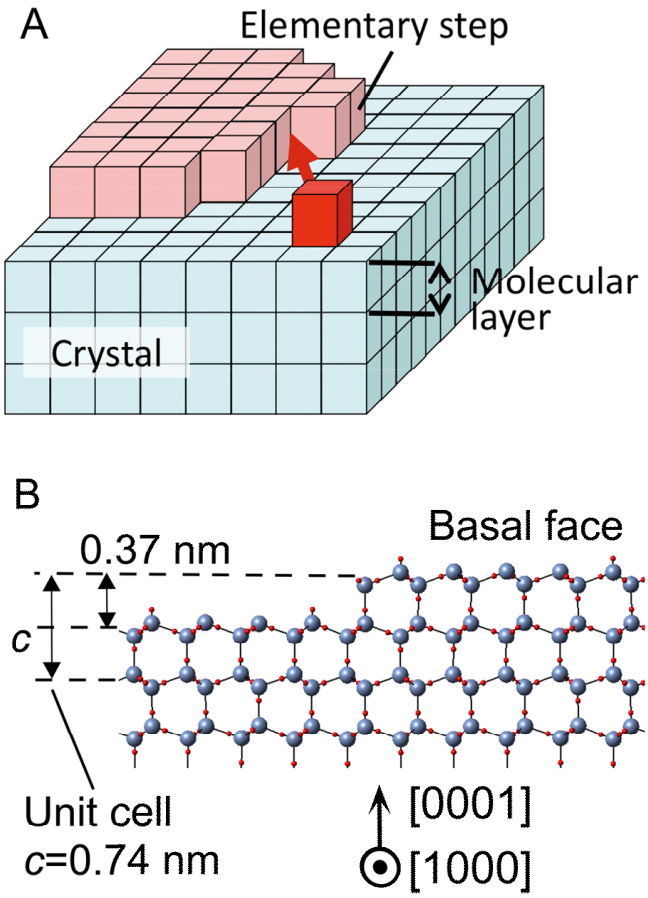

Fig. S4. Layer-by-layer growth of ice crystals and their elementary steps. A, A schematic illustration of the layer-by-layer growth. A crystal bounded by flat crystal faces grows layer by layer(30, 31), utilizing laterally growing molecular layers that have the minimum height determined by the crystal structure and the size of the molecules. A molecule (in red) coming from a surrounding phase jumps onto the ledge of the topmost molecular layer (in pink). Hence, growing ends of such molecular layers, so-called "elementary steps", which ubiquitously exist on a crystal surface, play a key role during many physical/chemical reactions on ice crystal surfaces, as well as the growth and sublimation/melting of ice crystals. B, A schematic drawing of a cross section of a Ih ice crystal. Gray and red atoms correspond to oxygen and hydrogen atoms, respectively. The half size of the unit cell in the *c* direction (0.37 nm) corresponds to the height of an elementary step on a basal face(7, 32).

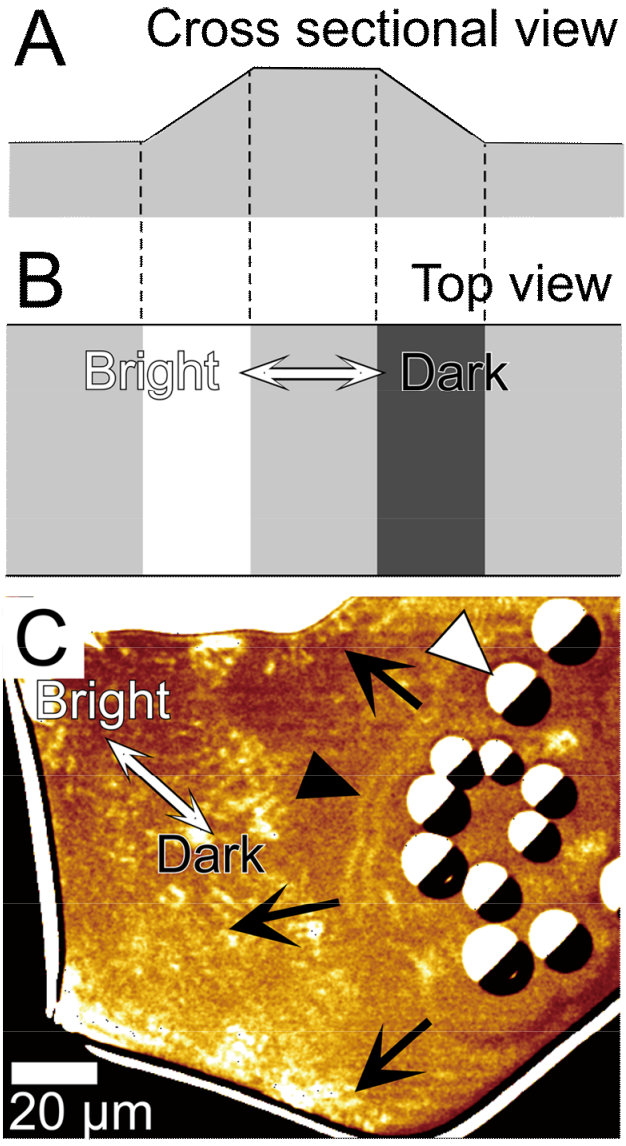

Fig. S5. Differential interference contrast. Utilizing interference of polarized light, differential interference contrast microscopy provides the contrast level so that slopes of one side and another side of a convex object look brighter and darker (white arrow), respectively, as schematically shown in A and B (as if a sample surface is illuminated from one slanted direction). Hence, in all LCM-DIM images shown in this study, the upper-left sides of the drops and steps look brighter and the lower-right sides of them look darker (a white arrow), as shown in C. In C, other arrows and arrowheads are the same as those in Fig. 1.

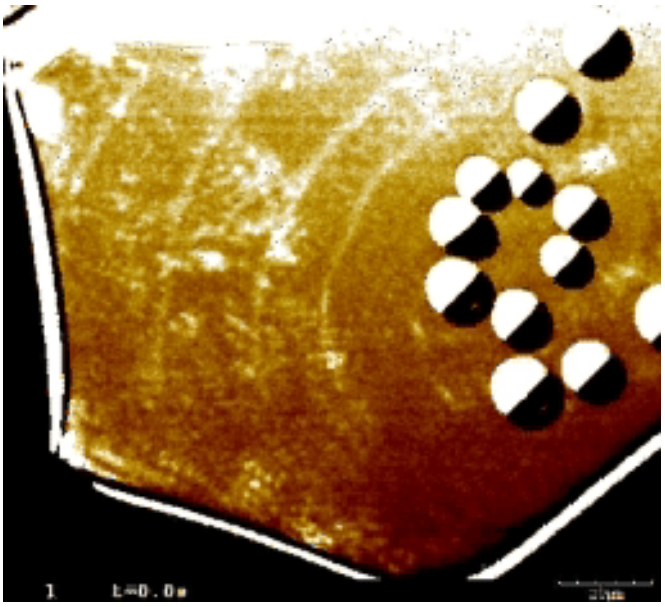

Video S1. The coalescence of round liquid-like droplets (α-QLLs) and the formation of elementary steps at -0.3°C (Figs. 1C and 2). Frame rate was 1.00 s/frame. Once α-QLLs had appeared, elementary steps appeared around them. To reduce the file size, the video file was converted from 512x466 pixels to 256x233 pixels.

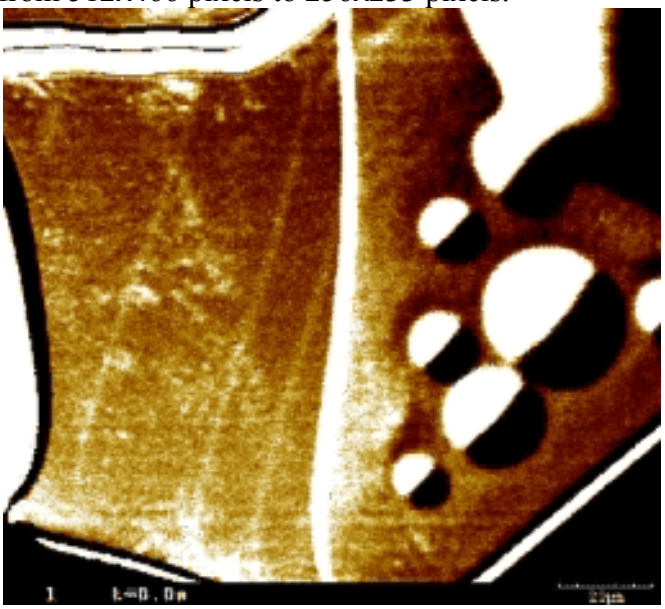

Video S2. The appearance of thin liquid-like layers (β-QLLs) in addition to round liquid-like droplets (α-QLLs) at -0.1°C (Figs. 3B and C). Frame rate was 1.00 s/frame. A bare basal face and growing elementary steps could be observed. In addition, two types of quasi-liquid layers formed by surface melting could be also observed simultaneously. We concluded from Fig. 5 (Video S3) that a thin liquid-like layer was not a solid phase but a quasi-liquid layer. To reduce the file size, the video file was converted from 512x466 pixels to 256x233 pixels.

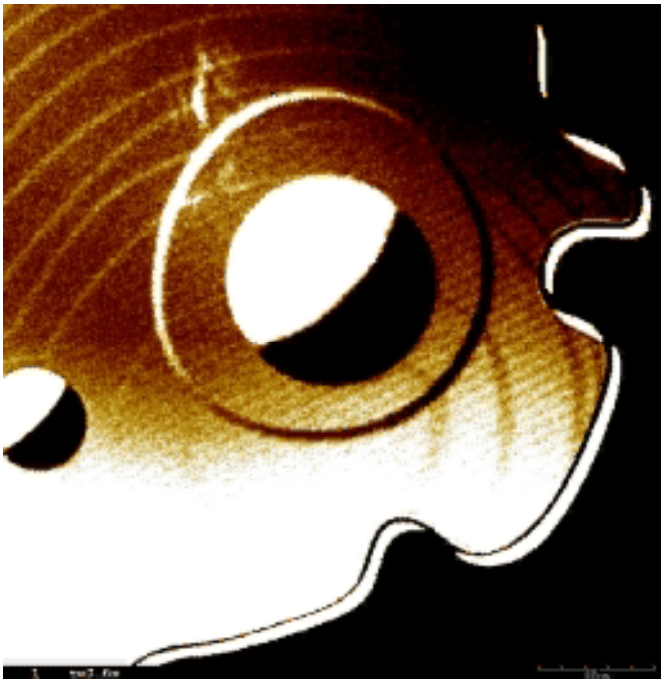

Video S3. Visualization of elementary steps growing beneath a β-QLL at -1.0°C (Figs. 5B and C). Frame rate was 3.27 s/frame. The gain and offset of LCM-DIM images were extremely adjusted to emphasize the contrast level of the images. An α-QLL is located at the center, and a β-QLL exists around the α-QLL. We could observe the growth of elementary steps even beneath the β-QLL, demonstrating that a β-QLL was a quasi-liquid layer. To reduce the file size, the video file was converted from 1,024x1,042 pixels to 256x262 pixels.

Video S4. Decomposition of a β-QLL into α-QLLs and solid ice with decreasing temperature (Fig. 6). After the appearances of α-QLLs and a β-QLL were confirmed at

-0.5°C, the temperature was decreased to -1.0°C. Frame rate was 3.27 s/frame. As time elapsed, a β-QLL was decomposed and changed into α-QLLs (small droplets) and bunched steps (solid ice). The decrease in the size of the α-QLL located at the center indicates that the α-QLL was also partly decomposed into solid ice. To reduce the file size, the video file was converted from 1,024x1,042 pixels to 256x262 pixels.

References

1. Petrenko VF & Whitworth RW (1999) *Physics of ice* (Oxford University Press, Oxford).
2. Wettlaufer JS & Dash JG (2000) Melting below zero. *Scientific American* 282(2):50-53.
3. Li Y & Somorjai GA (2007) Surface premelting of ice. *Journal of Physical Chemistry C* 111(27):9631-9637.
4. Faraday M (1850) Lecture given at Royal Institution, June 7, 1850. in *reported in Athenaeum*London), p 640.
5. Elbaum M, Lipson SG, & Dash JG (1993) Optical study of surface melting on ice. *Journal of Crystal Growth* 129(3-4):491-505.
6. Sazaki G*, et al.* (2004) In situ observation of elementary growth steps on the surface of protein crystals by laser confocal microscopy. *Journal of Crystal Growth* 262(1-4):536-542.
7. Sazaki G, Zepeda S, Nakatsubo S, Yokoyama E, & Furukawa Y (2010) Elementary steps at the surface of ice crystals visualized by advanced optical microscopy. *Proceedings of the National Academy of Sciences of the United States of America* 107(46):19702-19707.
8. Gonda T, Arai T, & Sei T (1999) Experimental study on the melting process of ice crystals just below the melting point. *Polar Meteorol. Glaciol.* 13:38-42.
9. Golecki I & Jaccard C (1977) The surface of ice near 0°C studied by 100 keV proton channeling. *Phys. Lett.* 63A:374-376.
10. Golecki I & Jaccard C (1978) Intrincis surface disorder in ice near melting-point. *J. Phys. C: Solid State Phys.* 11:4229-4237.
11. Frenken JWM, Maree PMJ, & Vanderveen JF (1986) Observation of surface-initiated melting. *Physical Review B* 34(11):7506-7516.
12. Pluis B, Vandergon AWD, Frenken JWM, & Vanderveen JF (1987) Crystal-face dependence of surface melting. *Physical Review Letters* 59(23):2678-2681.
13. Beaglehole D & Nason D (1980) Transition layer on the surface on ice. *Surface Science* 96(1-3):357-363.
14. Furukawa Y, Yamamoto M, & Kuroda T (1987) Ellipsometric study of the transition layer on the surface of an ice crystal. *Journal of Crystal Growth* 82:665-677.
15. Dosch H, Lied A, & Bilgram JH (1996) Disruption of the hydrogen-bonding network at the surface of I-h ice near surface premelting. *Surface Science* 366(1):43-50.
16. Kouchi A, Furukawa Y, & Kuroda T (1987) X-ray diffraction pattern of quasi-liquid layer on ice crystal surface. *Journal De Physique* 48(C-1):675-677.

17. Dosch H, Lied A, & Bilgram JH (1995) Glancing-angle X-ray scattering studies of the premelting of ice surfaces. *Surface Science* 327(1-2):145-164.
18. Lied A, Dosch H, & Bilgram JH (1994) Surface melting of ice I(h) single crystals revealed by glancing angle X-ray scattering. *Physical Review Letters* 72(22):3554-3557.
19. Maruyama M, Bienfait M, Dash JG, & Coddens G (1992) Interfacial melting of ice in graphite and talc powders. *Journal of Crystal Growth* 118(1-2):33-40.
20. Bluhm H, Ogletree DF, Fadley CS, Hussain Z, & Salmeron N (2002) The premelting of ice studied with photoelectron spectroscopy. *Journal of Physics-Condensed Matter* 14(8):L227-L233.
21. Nasson D & Fletcher NH (1975) Photoemission from ice and water surfaces: Quasiliquid layer effect. *J. Chem. Phys.* 62(11):4444-4449.
22. Kvlividze VI, Kiselev VF, Kurzaev AB, & Ushakova LA (1974) The mobile water phase on ice surfaces. *Surf. Sci.* 44:60-68.
23. Mizuno Y & Hanafusa N (1987) Studies of Surface Properties of Ice Using Nuclear Magnetic Resonance. *Journal de Physique C1* 3(48):511-517.
24. Kaverin A*, et al.* (2004) A novel approach for direct measurement of the thickness of the liquid-like layer at the ice/solid interface. *Journal of Physical Chemistry B* 108(26):8759-8762.
25. Sadtchenko V & Ewing GE (2003) A new approach to the study of interfacial melting of ice: infrared spectroscopy. *Canadian Journal of Physics* 81(1-2):333-341.
26. Bluhm H & Salmeron M (1999) Growth of nanometer thin ice films from water vapor studied using scanning polarization force microscopy. *Journal of Chemical Physics* 111(15):6947-6954.
27. Doppenschmidt A & Butt HJ (2000) Measuring the thickness of the liquid-like layer on ice surfaces with atomic force microscopy. *Langmuir* 16(16):6709-6714.
28. Salmeron M & Bluhm H (1999) Structure and properties of ice and water film interfaces in equilibrium with vapor. *Surface Review and Letters* 6(6):1275-1281.
29. Corle TR & Kino GS (1996) *Confocal scanning optical microscopy and related imaging systems* (Academic Press, London).
30. Chernov AA (1984) *Modern crystallography III* (Springer-Verlag, Berlin).
31. Markov IV (1995) *Crystal growth for beginners* (World Scientific, Singapore).
32. Zepeda S (2004) Intermolecular interactions: from the hydrogen bond to biological function. Ph.D. (University of California, Davis).